



Electrochemical leaching of spent LIBs: Kinetics, novel reactor, and modeling

July 2024

Changing the World's Energy Future

Daniel Ernesto Molina Montes de Oca, Meng Shi, Luis A Diaz Aldana, Tedd Lister



DISCLAIMER

This information was prepared as an account of work sponsored by an agency of the U.S. Government. Neither the U.S. Government nor any agency thereof, nor any of their employees, makes any warranty, expressed or implied, or assumes any legal liability or responsibility for the accuracy, completeness, or usefulness, of any information, apparatus, product, or process disclosed, or represents that its use would not infringe privately owned rights. References herein to any specific commercial product, process, or service by trade name, trade mark, manufacturer, or otherwise, does not necessarily constitute or imply its endorsement, recommendation, or favoring by the U.S. Government or any agency thereof. The views and opinions of authors expressed herein do not necessarily state or reflect those of the U.S. Government or any agency thereof.

Electrochemical leaching of spent LIBs: Kinetics, novel reactor, and modeling

Daniel Ernesto Molina Montes de Oca, Meng Shi, Luis A Diaz Aldana, Tedd Lister

July 2024

**Idaho National Laboratory
Idaho Falls, Idaho 83415**

<http://www.inl.gov>

**Prepared for the
U.S. Department of Energy
Under DOE Idaho Operations Office
Contract DE-AC07-05ID14517**

Electrochemical leaching of spent LIBs: Kinetics, novel reactor, and modeling

Abstract

The use of electrons as main reagent for the recovery and recycling of critical metals from spent lithium-ion batteries (LIBs) is a process electrification strategy that can be used to close the life-cycle loop of LIBs through more sustainable methods. Electrochemical leaching, a process that uses a reductant that is constantly regenerated electrochemically for the leaching of lithium-ion battery black mass (LIBBM), has shown high extraction efficiencies and sustainable scores. However, slow kinetics, reactor design challenges and lack of deeper understanding of the underlying processes are barriers to the optimization, scale-up, and market adoption of this technology. A kinetic study and mathematical model for dissolving LIBBM is presented to better understand the underlying mechanisms aiming to reduce the processing time and make predictions for future design and scale-up. The effect of acid and electrochemically mediated reductant concentrations, LIBBM loading, and cathode/reactor designs were explored. As a result, the leaching time was reduced from 7 h to under 1 h at a pulp density of 73 g/L, without external heating. A novel reactor with parallel baffle electrodes (PBE) was developed, which significantly reduced the leaching time by improving convection in a stirred slurry electrochemical reactor. Dimensionless numbers were deduced from an unsteady state model, which can be used in dimensional analysis for future process design and scale-up.

Keywords

Lithium-ion Battery Recycling, Electrochemical Leaching, Kinetic Analysis, Parallel Baffle Electrode, Dimensionless Model, Electrochemical Reactor

1. Introduction

The fast growing amount of end-of-life lithium-ion batteries (LIB) used in consumer electronics, electric vehicles (EV) and stationary energy storage, requires the development of sustainable recycling strategies addressing environmental concerns associated with its disposition, but also critical materials supply chain challenges [1, 2]. The development and adoption of more efficient and sustainable hydrometallurgical processes in LIB recycling is key, as a replacement or complement to pyrometallurgical processes, which are traditionally less efficient, recover less materials and have higher environmental impact [3, 4].

Leaching is a key unit operation in hydrometallurgy, where the metals are extracted in a concentrated liquor to continue subsequent separation and purification steps. The active materials from spent LIBs contain mixed oxides of valuable metals Li, Ni, Mn, and Co that are insoluble in aqueous media and are difficult to leach in acid alone at their higher oxidation states of Ni^{3+} , Co^{3+} and Mn^{4+} [5]. To attain high leaching efficiencies above 90% and industry-relevant reaction rates, acid, chemical reductant, and often heating, are needed [6-8], with H_2O_2 being the most commonly reported reductant [9, 10].

Electrification has been identified among one of the main strategies to achieve a more sustainable hydrometallurgy, or “circular metallurgy” [4]. If the electrons are derived from low carbon energy, the sustainability of the process increases [11]. Approaches that use the LIB cathodes or LIBBM directly as the cathode material for the reduction and dissolution of metals have been investigated with low chances for scale-up due to their intrinsic low throughput limitations [12-16]. On the other hand, the use of electrochemically generated redox mediators

46 better follows the operation of what established hydrometallurgical processes do. Furthermore,
47 common reducing/oxidizing chemicals that are toxic or have a large carbon footprint, such as
48 SO_2 and H_2O_2 [11], can be replaced with more benign redox mediators that can be regenerated
49 electrochemically.

50 Iron (II) has been reported to be a good reductant for LIBBM leaching [17-20], and the expected
51 reductive leaching reaction in the presence of Fe^{2+} and acid is:

52
53 with $x+y+z = 1$. Iron has the advantage of not being toxic and that is already present as an
54 impurity in shredded LIBMM. Instead of using a stoichiometric or excess amount Fe^{2+} , Porvali
55 et al.[17, 18], Chernyaev et al.[21], and Peng et al.[22], demonstrated that sub-stoichiometric
56 amounts of this reductant, in the range of 0.02-0.05 mol Fe/mol LiCoO_2 , can be regenerated by
57 galvanically reducing Fe^{3+} with Cu or Al metal particles. By contrast, in previous work [23], the
58 regeneration of Fe^{2+} , also in sub-stoichiometric concentration, was achieved electrochemically at
59 a cathode's surface (Equation 2), achieving >96% leaching of Co, Ni, Mn, and Li from
60 commercial LIBBM in a stirred electrochemical cell. This process operates at ambient
61 temperature, while using moderate sulfuric acid concentrations (0.5-2 M), low reductant
62 concentration (10 mM Fe^{2+}) and high pulp densities between 65 and 240 g/L [23].

63
64 Moreover, the LIBBM contains impurities from metallic components in the shredded batteries,
65 such as Al, Fe and Cu. This process removes Cu concurrently through electrowinning. Although
66 electrowinning on a cathode is an established method of copper recovery, it had not been
67 combined with leaching in a single operation before.

68 This type of electrochemical regeneration of iron as a redox mediator has also been reported for
69 Electro-Fenton water treatment applications [24, 25], and for the leaching of manganese and
70 cobalt oxides from mining ores [26].

71 Despite these advantages, the kinetics of electrochemical leaching are low and required nearly
72 seven hours to complete at the lowest pulp density of 65 g/L and 7.7 mol of H_2SO_4 /kg LIBBM.
73 Longer leaching time means larger equipment, which is reflected in a higher capital cost [23].
74 For scale up and market adoption of this technology, the leaching rate needs to be improved
75 dramatically while maintaining its sustainability advantages. A better understanding of the
76 underlying processes in electrochemical leaching and improved reactor design are necessary to
77 accomplish this goal.

78 In this work, a kinetic study of electrochemically assisted leaching of cobalt-rich LIBBM was
79 performed to identify the limitations for fast leaching and to build a mathematical model that can
80 be implemented in simulations for future reactor design and process scale-up. We developed a
81 reactor with a novel Parallel Baffle Electrode design, which solves several challenges for stirred
82 slurry electrochemical tank reactors that use a membrane. With this design and new operating
83 conditions, the leaching time was decreased by 88% with respect to previous work [23]. A
84 dimensionless mathematical model was deduced that can reasonably predict the observed
85 currents and leaching times when solved numerically as well as provide quick estimation of the

86 effect of process parameters using dimensionless analysis from the model.

87 **2. Materials and Methods**

88 The stirred tank is a common reactor for contacting solid particles in suspension with leaching
89 agents [27]. An in-house-made, two-compartment, stirred electrochemical cell was used for this
90 study. The cathode compartment, a 250 mL squared shaped polypropylene chamber, was
91 separated from the 60 mL anode chamber by a bipolar membrane (FBM-PK, Fumasep). Figure 1
92 shows a diagram of the cell and its different variations, and Figure S2 of the Supplementary
93 Information shows photos of the cell. A 38-mm diameter, 4-blade 45°-pitched blade impeller
94 made of PTFE (A185, Caframo), was used to stir the slurry at rotation rates between 700 and 800
95 rpm. The cathodes were 304 stainless-steel 40 mesh (0.011" diameter), coupons cut in different
96 configurations and sizes. A single 33 cm²-immersed area flat coupon, shown in Figure 1A and
97 S2A, was used as the baseline comparison based on the configuration reported in our previous
98 work [23]. Then segmented cathodes arranged in "radial baffles" (Figure 1B, and S2B), and
99 ultimately in "parallel baffles" (Figure 1C and S2C) were tested as improved configurations.

100 The leaching experiments were performed using cobalt rich LIBBM provided by Cirba Solutions
101 (Trail, British Columbia, Canada) with a composition shown in Table 1. Pristine LiCoO₂ or
102 LiNi_{1/3}Co_{1/3}Mn_{0.1/3}O₂ (MTI, Richmond, CA) was also used were specified. Sulfuric acid (95-98
103 wt.%, certified ACS Plus A300-212, Fisher Chemical), nitric acid (certified ACS Plus
104 A-200-212, Fisher Chemical), hydrochloric acid (certified ACS Plus A-144-212, Fisher
105 Chemical), KOH (90% reagent grade 484016 Sigma-Aldrich) and ferric sulfate heptahydrate
106 (99+% ACS reagent 423735000 Thermo Scientific) were used. Leaching was performed in 0.18
107 L of 0.5 - 2 M H₂SO₄ solution. The initial concentration of reductant Fe²⁺ was 0.010 - 0.04 mol/L
108 prepared in nano-pure water (18MΩ, PURELAB Flex 1). The anode was formed with two back-
109 to-back rectangular IrO₂/Ti meshes, with a face area of 2×35 cm². The anolyte solution was 2 M
110 KOH.

111 A voltage of -2.1 VDC was applied using a potentiostat (Solartron 1286 or Biologic SP-50), or a
112 Power Supply (Siglent SPD1168X) to record the current profiles. This voltage was chosen to
113 obtain cathodic limiting currents for Fe(III) and Cu(II) reduction during leaching; it
114 approximates the measured voltage for previously reported electrochemical leaching at a
115 controlled potential of -0.3 V vs Ag/AgCl [23]. Constant voltage operations are more industrially
116 applicable than a controlled potential. The current profile was followed to identify the end point
117 of the leaching process. At this point the current curve transitions to a background current, where
118 prior work showed over 96% dissolution of Ni, Co, Mn, and Li. There was no external heating
119 but, in some cases, the initial temperature increased from ambient to 30-40 °C due to sulfuric
120 acid enthalpy of dissolution and temperature decreased less than 3 °C during leaching due to heat
121 generation from ohmic resistance to the current and heat losses to the surroundings.

122 An atomic absorption spectrometer (Agilent, 240FS AA) was used to determine the
123 concentration of metals in the leachate and undissolved materials following digestion in aqua
124 regia. The composition of the LIBBM and two examples of leached LIBBM are shown in Table
125 1. A previous publication [23] contains an XRD diffractogram showing the different phases of
126 battery materials found in this LIBMM.

127 **Table 1.** Composition of the LIBMM and two examples of electrochemical leaching using radial
 128 baffle electrodes at room temperature, with 73 g/L of LIBBM, 1 M H₂SO₄ solution and voltage
 129 of 2.1V. The corresponding current profiles appear in Figures 3A and S3. SEM and SEM-EDS
 130 images and analysis for the LIBMM and undissolved material are shown in Figures S4-S9.

Element	LIBBM	Electrochemical leaching with 10mM		Electrochemical leaching with 40mM	
		Fe, 3-baffle cathode with 16.9 cm ²		Fe, 4-baffle cathode with 26.1 cm ²	
		area		area	
		Undissolved material	Efficiency	Undissolved material	Efficiency
	wt.%	wt.%	%	wt.%	%
Li	2.79	0.189	97.88	0.081	99.14
Cu	0.34	0.002	99.78	0.007	99.42
Al	0.46	0.244	83.33	0.496	68.00
Mn	4.23	0.219	98.38	0.069	99.52
Fe	0.43	0.171	87.63	0.165	88.67
Co	12.20	0.743	98.09	0.278	99.33
Ni	7.48	0.555	97.67	0.333	98.68
Zn	0.09	0.005	98.32	0.004	98.86

131

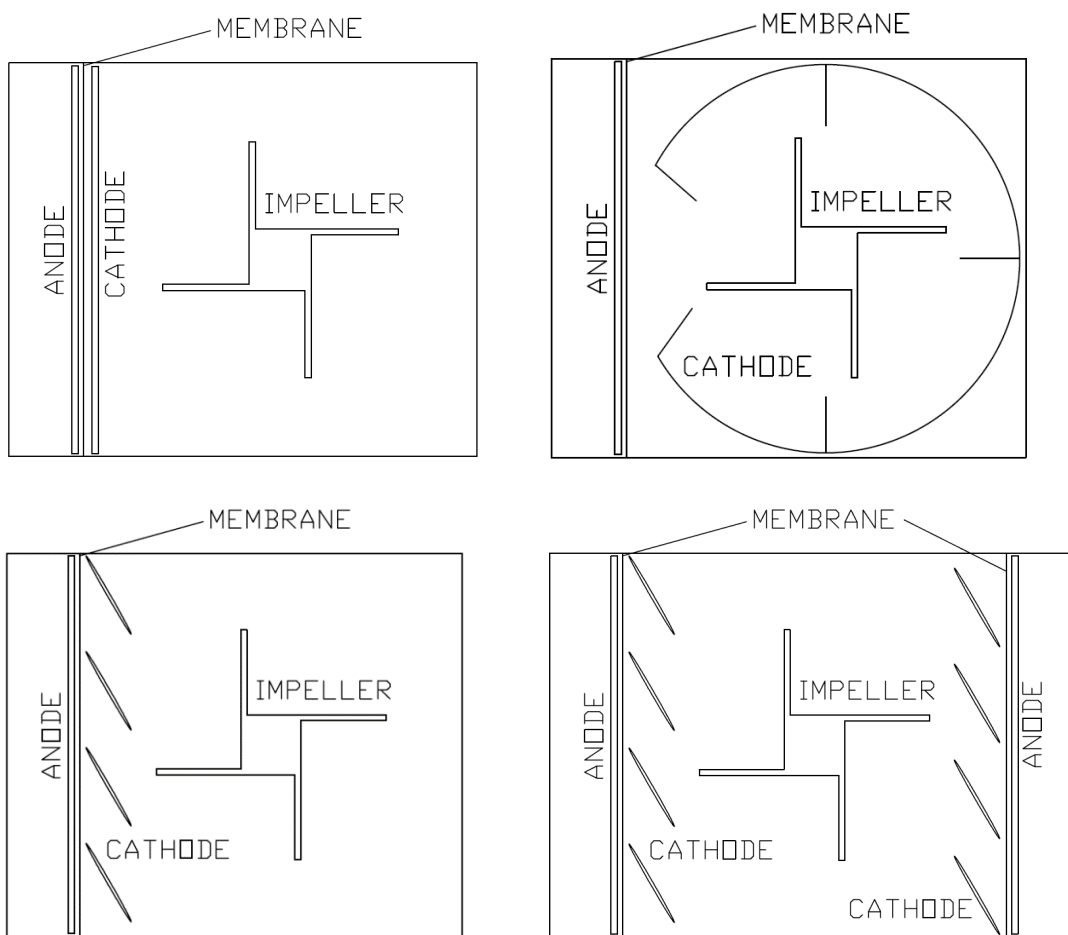
132 3. Results and Discussion

133 Initially, a flat metallic mesh cathode (Figure 1A and S1A) was used in the stirred
 134 electrochemical reactor as previously reported [23], but this set up showed unstable currents,
 135 poor convection, and LIBBM accumulation on one side of the cathode. Moreover, at speeds
 136 above 400 rpm, a hydrodynamic vortex formed around the impeller. In mixed tanks, dead zones
 137 need to be avoided and baffles are typically installed to suppress hydrodynamic vortices [28, 29].
 138 Thus, a new segmented cathode design was implemented, so that it would function both as an
 139 electrode and baffle while avoiding LIBBM accumulation. Previously, Yanez-Varela et al.
 140 demonstrated the advantage of tubular cathode-anode electrode pairs that doubled as baffles in a
 141 stirred electrochemical reactor without membranes [30]. Different iterations of the baffle radial
 142 electrode design were employed, including cathodes with 3, 4 and 5 baffles; the 5-baffle radial
 143 electrode is shown in Figure 1B and S2B. The leaching efficiencies for 3 and 4-baffle radial
 144 cathode experiments are shown in Table 1. The rest of the experiments had leaching efficiencies
 145 that were above 97%.

146

147

148
149
150
151
152
153
154
155
156
157
158
159
160
161
162
163
164
165
166
167
168
169
170
171
172
173



174
175
176
177
178

Figure 1. Top view diagrams of the electrochemical cells used in this study: with a flat cathode (A, upper left), radial baffle electrode (B, upper right), Parallel Baffle Electrode (PBE) (C, lower left), dual PBE (D, lower right). The PBE-Membrane-Anode combination is repeated in the case of the dual cathode reactor. The pitched-blade impeller rotates clockwise and creates axial and radial flow of the slurry.

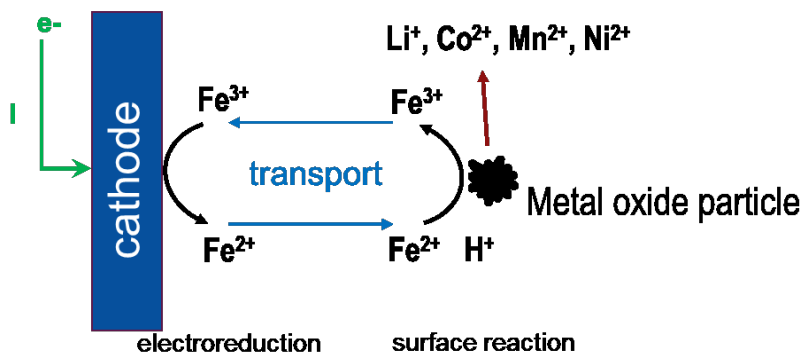
179 3.1 Kinetic Study

180 The main processes occurring in the reactor during electrochemical leaching are shown in Figure
181 2. Pourbaix or E-pH diagrams (Figure S1 in Supplementary Information) for a representative
182 LiCoO_2 LIB material predict that under reductive potentials and acid conditions, transformation
183 of the insoluble cobalt oxide to the “free” divalent ion in solution is thermodynamically favored.
184 The results in Table 1 and the SEM analysis of the LIBBM and remaining solid (S4-S9) confirm
185 the dissolution of the active particles that contain Co, Ni, Mn. This, however, does not give any
186 information about the kinetics and mechanism of the process; thus, we study leaching kinetics in
187 this section.

188 A radial baffle electrode, like the one shown in Figure 1B but with 3 baffles, was used, with a
189 submerged face area of 16.9 cm^2 . The leaching efficiencies are shown in Table 1 and the current
190 profile during leaching, at an applied voltage of 2.1 V, is shown in Figure 3. The catholyte was

191 used at a room temperature of $\sim 22^\circ\text{C}$ and had an initial reductant concentration of 10 mM Fe^{2+}
 192 and an acid concentration of $1\text{ M H}_2\text{SO}_4$, the latter being in excess of the 0.45 M stoichiometric
 193 amount needed for the leaching of 73 g/L of black mass. Part of the acid is consumed right upon
 194 mixing with the black mass, and a moderate excess of acid remains in solution for a final pH of
 195 $0.3\text{-}0.4$. Porvali et al.[18] and Cerrillo-Gonzalez et al.[9] showed high leaching efficiencies and
 196 kinetics at $1\text{ M H}_2\text{SO}_4$, and demonstrated that in the presence of a reductant, a large excess of
 197 sulfuric acid beyond 1 M does not provide significant improvement, and can even hinder the
 198 kinetics at a high concentration of 3 M .

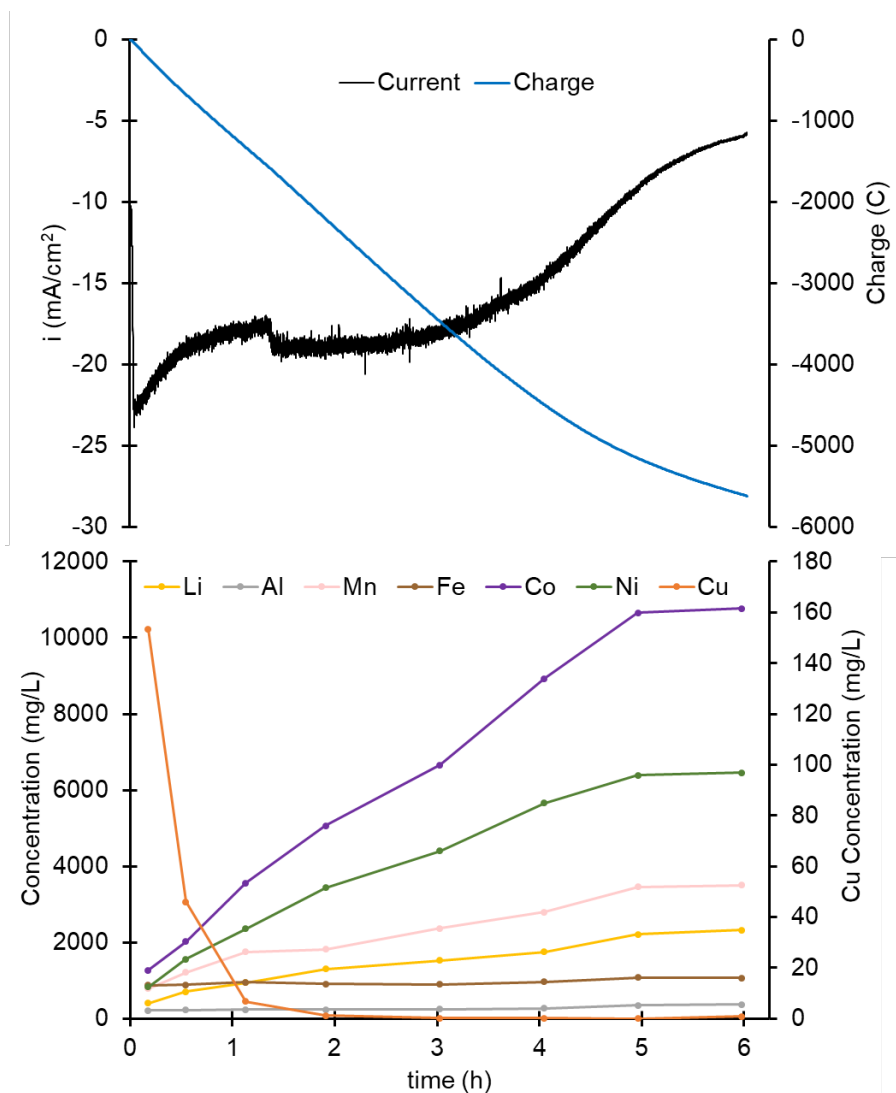
199



200

201 **Figure 2.** Electrochemical leaching process diagram showing the main electrode reaction, mass
 202 transport, and surface reaction on the leaching particle.

203 Before LIBBM is added, the cathode is polarized in the sulfuric acid-ferrous sulfate solution,
 204 obtaining a background current of $\sim 173\text{ mA}$, which is expected to be mostly from hydrogen
 205 evolution reaction (HER). Upon addition of LIBBM, the steep increase in the current is due to an
 206 increase in Fe^{3+} from the reaction in Equation 1. This is also observed when pristine LiCoO_2 or
 207 $\text{LiNi}_{1/3}\text{Co}_{1/3}\text{Mn}_{0.1/3}\text{O}_2$ particles are used instead of LIBBM (not shown). The current passes
 208 through a maximum and then starts to decrease. The current profile remains almost flat between
 209 1-3 hours of leaching, indicating a pseudo-steady state where the total reduction rate at the active
 210 particles is close to the total reduction rate at the cathode. We can estimate this rate to be 3.4
 211 $\mu\text{mol/s}$ for a single-electron reduction at a current of 0.325 A . At the end of the pseudo-state
 212 region the current drops, indicating a decrease in the Fe^{3+} concentration, as less cathode material
 213 is available for reaction. A lower Fe^{3+} concentration implies a higher Fe^{2+} concentration, which
 214 will increase the surface-specific reaction rate ($\text{mol/m}^2\text{s}$), at the cathode LIBBM particles. Figure
 215 3A also shows the integrated current. i.e., electric charge, with a total charge of $\sim 5600\text{ C}$ by the
 216 end of the leaching process, which includes the background current.



217

218 **Figure 3.** Current-charge (A, top) and concentration (B, bottom) leaching curves for LIBBM in
 219 1 M H₂SO₄ and 0.010 M Fe₂SO₄ at -2.1 V. Bottom: Early removal of copper is evident, as well
 220 as an approximately linear ($r=0.99$) curve for Co and Ni and near completion of leaching by 5
 221 hours. The total charge at near leaching completion of metal Co, Ni and Mn (98%) is about 5600
 222 C. The sudden change in current at 1.3 h was due to accidental movement of the cathode. The 3-
 223 baffle radial cathode area was 16.9 cm² and the stirring speed 688 rpm.

224 The metals' concentration profiles during leaching are shown in Figure 3. Metallic copper
 225 present as impurity acts as a galvanic reductant and is dissolved by Fe³⁺[31] as shown in
 226 Equation 3:

227

228 Most of the copper is removed within the first hour of leaching by plating on the cathode, with a
 229 final removal efficiency of 99%. Instead of the commonly reported sigmoidal shape for reductive
 230 leaching curves [10], the concentration versus time curve for Co and Ni are close to linear
 231 ($r=0.99$) for up to 5 hours, after which the concentrations remain almost constant with a slight

232 increase of less than 2% by the end of the leaching. A similar linear behavior is reported by
233 Ferron et al. during the electrochemical leaching of MnO₂ ores [26]. A near complete leaching of
234 the active material (98%) is obtained before the current completes transitions to a background
235 current, or the charge curve transitions to a straight line of lower slope as shown in Figure 3.

236 To proceed with the kinetics analysis, a shrinking spherical particle model [32, 33] is applied to
237 conversions derived from Figure 3, assuming a constant surface reaction rate r' as shown in
238 Equation 4:

239

240 If the leaching rate is controlled by the surface reaction on the LIB cathode particles, then
241 Equations 5-6 apply:

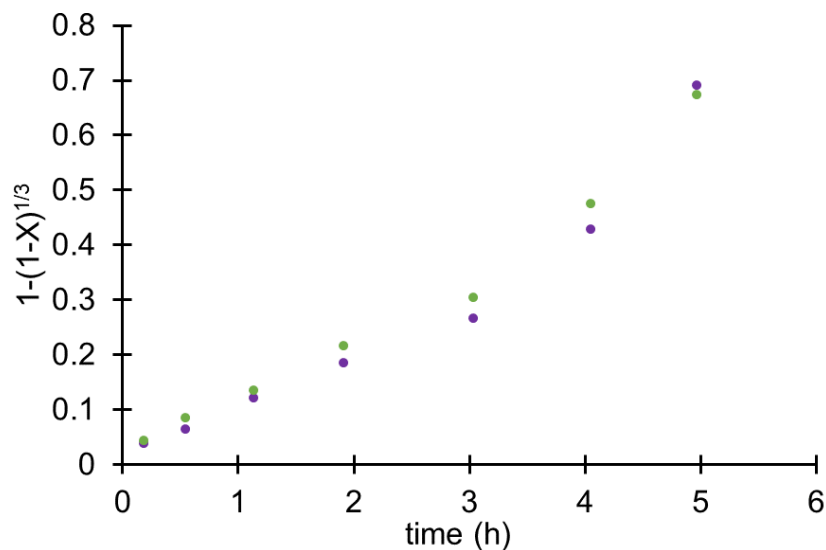
242

243

244 Equations 5-6 assume a constant reductant concentration. Figure 4 shows a good linear fit to the
245 model for Co and Ni during the first 3 hours of leaching ($r = 0.999$), after which the slope of the
246 curve increases. This behavior could be explained by a relatively constant, low concentration of
247 the reductant Fe²⁺ during the first 3 hours of leaching. The reductant concentration is expected to
248 increase as the total surface area of the particles decreases with time, causing the surface reaction
249 rate r' (mol/m²s) to increase. This behavior is similar to the one reported by Porvali et al. for
250 LiCoO₂ [17], where there is a linear section of lower slope during the first 25% of the leaching,
251 and another of higher slope for the rest of leaching. The linear fit for $t \leq 3$ h produces a value of
252 $1.4 \times 10^{-3} \text{ min}^{-1}$ ($r = 0.999$), which is in the same order of magnitude as the constants reported by
253 Porvali et al.[17] ($3\text{-}8 \times 10^{-3} \text{ min}^{-1}$ at 30°C) for the leaching of LiCoO₂ at similar concentrations of
254 acid and iron, but using metallic copper as galvanic reductant instead of electricity. The galvanic
255 reduction has the drawback of requiring the addition of a mass of metallic copper of at least one
256 third of the mass of active particles, which then needs to be removed from the solution. The fit to
257 the surface reaction-controlled model was confirmed against the film diffusion-control model
258 using multiple regression as described by Faraji et al.[34].

259 From the estimated value of $1.4 \times 10^{-3} \text{ min}^{-1}$ and Equation 6 we can calculate a value for the first
260 order surface kinetic constant $k_r = 3 \times 10^{-6} \text{ m/s}$, with $\rho = 0.0456 \text{ mol/cm}^3$, $R = 5 \text{ }\mu\text{m}$ for typical
261 NMC particles and $C_{\text{Fe}^{2+}} = 0.16 \text{ mM}$ (1/10 of the estimated iron concentration). This value of k_r is
262 in the same order of magnitude ($8 \times 10^{-6} \text{ m/s}$) when compared to the square root of a second order
263 k_r for the reduction of LiCoO₂ with H₂O₂ used in a model by Cerrillo-Gonzalez et al.[9].

264



265
 266 **Figure 4.** Shrinking particle model curves for the leaching in Figure 3. There is a good linear fit
 267 ($r=0.999$) up to 3 hours of leaching for both Co and Ni.

268 When the relative velocity and the size of the active particles is such that mass-transfer
 269 limitations are overcome, then the leaching process will be surface kinetics-limited [35]. With
 270 the calculated k_r value, the critical particle size or threshold radius below which the surface
 271 reaction kinetics dominate over diffusion can be calculated with Equation 7 [33]:

272
 273 With a diffusion coefficient, D , reported to be $5 \times 10^{-10} \text{ m}^2/\text{s}$ for Fe^{2+} [36], we obtain $r_{crit} = 1.25 \times 10^{-4}$
 274 m. This radius is at least one order of magnitude larger than the active particles in the LIBMM
 275 (see Figure S4), which implies that the rate limiting step is likely to be the surface reaction.
 276 Porvali et al.[17, 18], Gao et al.[10], Li et al.[37], Li-Po et al.[38], Sun et al.[8] also found the
 277 reductive leaching of LIBBM to be surface kinetic-limited by fitting the conversion to a
 278 shrinking particle model. Leaching of pristine LiCoO_2 performed without any applied current at
 279 two different mixing speeds, 400 and 700 rpm, produced the same leaching profile for both
 280 conditions (Figure S10). This confirms that at the mixing speeds used, the leaching kinetics is
 281 not controlled by mass transfer but by the surface reaction. This concurs with the findings by Li-
 282 Po [38], where beyond 400 rpm there is no change in the leaching efficiency with the stirring
 283 speed.

284 If the leaching of particles is surface reaction limited, the strategies to decrease leaching time
 285 include an increase in $k_r(T)$ or $C_{\text{Fe}^{2+}}$, or the particle size must be reduced. Since LIBBM has
 286 already been through a grinding operation by the supplier, size reduction was not studied. The
 287 leaching reaction rate can be increased by increasing the temperature, but heating was not
 288 considered to avoid additional energy consumption. Then, the concentration of reductant $C_{\text{Fe}^{2+}}$
 289 during leaching can be increased by increasing its initial concentration, or by improving the
 290 regeneration rate at the cathode.

291 Besides homogenizing the slurry and promoting mass transfer around the leaching particles,
 292 convection in the reactor affects mass transfer on the cathode surface. A higher convection

293 decreases the diffusion layer thickness [39] and increases the flux of iron and copper ions to the
294 electrode surface, thus increasing the current. The total rate at which the redox agent is
295 regenerated in the reactor is critical to maintaining the concentration of reductant as high as
296 possible. The highest mass flux is achieved at limiting current [40], which depends on the
297 concentration of the species being reduced and the global mass-transfer coefficient. The mass
298 transfer coefficient depends, in turn, on the flow of electrolyte in the reactor [41], and shorter
299 times to full conversion have been reported at higher mixing speeds [30].

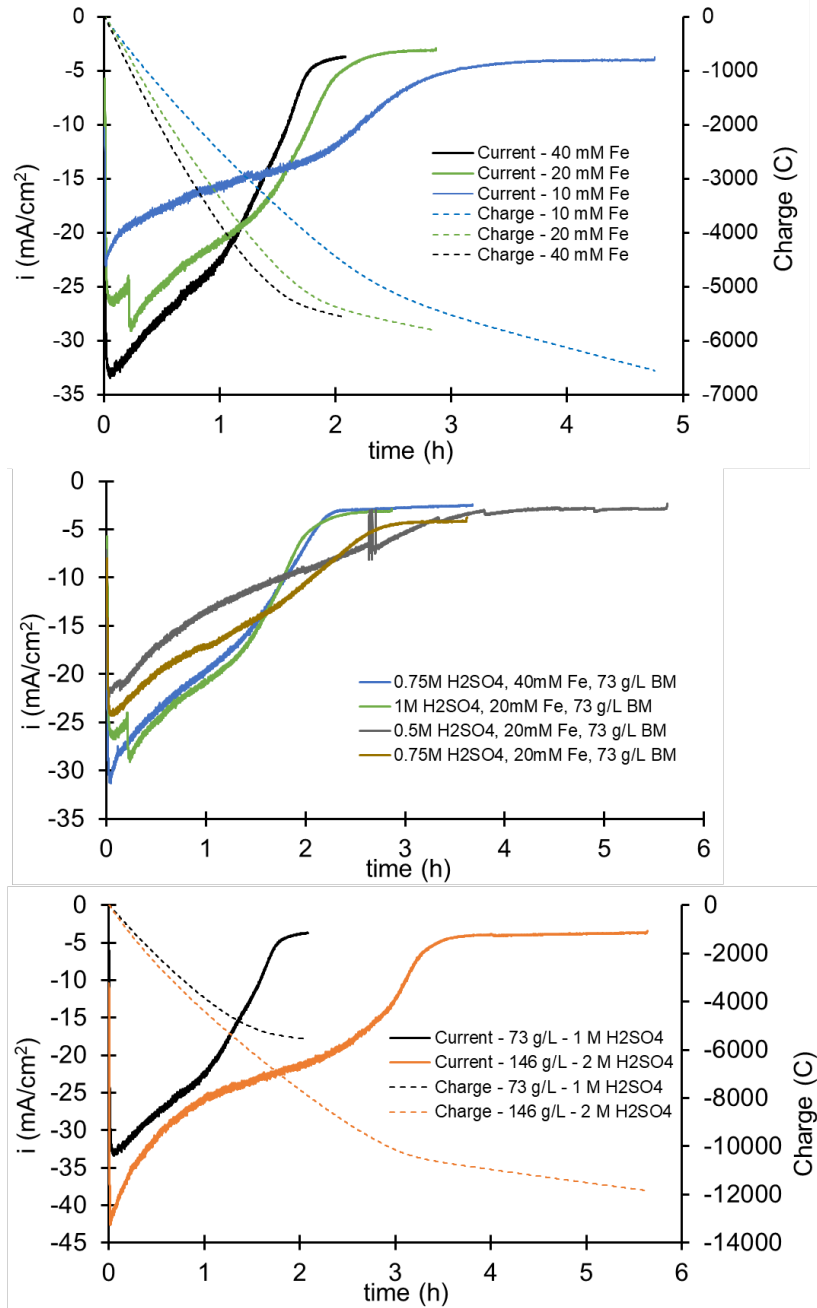
300 If we calculate the Reynolds number with Equation 8, at 400 and 700 rpm, we obtain 9700 and
301 17000, respectively:

302
303 Where N is the stirring speed (6.67 or 11.7 1/s), D is the impeller diameter (0.0381 m) and σ is
304 the kinematic viscosity (1×10^{-6} m²/s). These Reynold numbers correspond to a turbulent regime
305 for water; an increase in the viscosity a slurry up to 200% from water would still fall under a
306 fully turbulent regime for the operating speed of 700 rpm, with higher viscosities falling under a
307 transitional flow between turbulent and laminar.

308 **3.2 Leaching at different conditions**

309 A 5-segment radial baffle cathode design, shown in Figure 1B, was used, with a submerged face
310 area of 38.5 cm². To increase the temperature without external heating, concentrated sulfuric acid
311 solution was diluted in the reactor to form the leaching solution right before each experiment. An
312 increase of 12 °C is observed when the 1M sulfuric acid solution is prepared in the reactor, which
313 is about 5 °C lower than what is predicted according to the heat of dilution reported in the
314 literature [42], and can be explained from the heat transfer to the surroundings. Different
315 concentrations of sulfuric acid, ferrous sulfate and LIBBM were explored as shown in Figure 5.
316 All these experiments have a similar charge of ~5500 C per 73 g/L, up to the time when the
317 current transitions to a background current. Figure 5A shows the effect of initial ferrous sulfate
318 concentration. Going from 10 to 20 mM increased the observed current and reduced the leaching
319 time by ~35%, but the effect is less pronounced when going from 20 to 40 mM. Initial
320 concentrations above 40mM of Fe²⁺ were not used to avoid overloading the downstream
321 impurity removal steps [43].

322



323

324 **Figure 5.** Current curves during leaching at different conditions with a 38.5 cm² radial baffle
 325 cathode at 2.1 V **(A, top)** Leaching at different ferrous sulfate concentrations in 1M H₂SO₄ and
 326 73 g/L of LIBBM. The highest reductant concentration shows a shorter time to reach the
 327 transition to background current, but similar total charge of ~5500 C. **(B, middle)** Leaching at
 328 different sulfuric acid concentrations. The 0.5 M H₂SO₄ case needed additions of 4M H₂SO₄
 329 solution to maintain the pH below 2 **(C, bottom)** Leaching at different LIBBM pulp densities
 330 while maintaining a constant acid/LIBBM ratio, FeSO₄ concentration of 40 mM. The total
 331 charge to the end of the inflection is about 5500 C and 11000 C, respectively.

332 The effect of the initial acid concentration is shown in Figure 5B. An initial concentration of 0.5
333 M H₂SO₄ is under-stoichiometric, and was insufficient to maintain the pH below 2, thus, further
334 additions of 4M H₂SO₄ were necessary, consistent with the previous paper on this method [23].
335 Although this mode of operation achieves a leaching efficiency above 98%, it leads to lower
336 currents and longer leaching times. The leaching curve for 0.75 M H₂SO₄ with 40 mM Fe is very
337 similar to 1M H₂SO₄ with 20 mM, so that in this case an increase in the reductant concentration
338 allowed the use of less acid without losing performance. A ratio of 13.7 mol of H₂SO₄/kg of
339 LIBBM (1M H₂SO₄ to 73 g/L) provided the fastest leaching in the range tested. The same moles
340 of acid per kilogram of LIBBM are kept for the runs in Figure 5C, where a higher black mass
341 loading was explored. In this case the leaching time and charge roughly doubled.

342 **3.3 Parallel Baffle Electrode (PBE)**

343 The radial baffle electrode design around the center of the reactor prevents the formation of a
344 vortex and stagnation of slurry, but it is highly asymmetric with respect to the membrane/anode,
345 so it was re-designed. The asymmetry and separation of several centimeters to the anode of some
346 of the radial baffles generate a distribution of ohmic drop, so that the baffles farthest from the
347 membrane will see a less cathodic electrochemical potential due to higher ohmic drop. To
348 prevent this, a new Parallel Baffle Electrode design was implemented, as shown in Figure 1C
349 and 1D. The separation between anode and cathode is of concern, since due to ionic ohmic
350 resistance there is a loss of voltage that needs to be minimized to decrease the power
351 consumption of the reactor [44, 45].

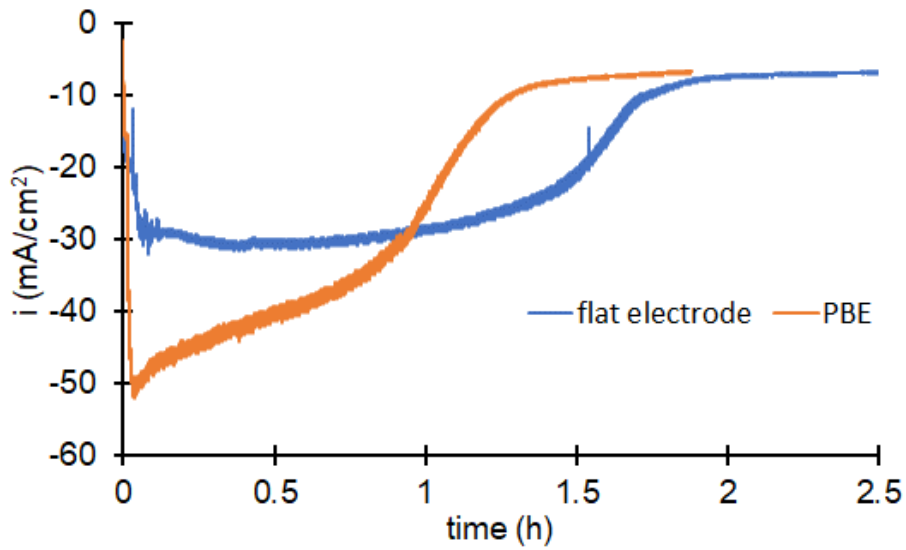
352 The new segmented cathode design has the following advantages, the majority of which are a
353 combination from the flat and the radial baffle electrodes:

- 354 1. The cathode segments double as baffles for a stirred reactor, disrupting the formation of a
355 hydrodynamic vortex and improving mixing.
- 356 2. It is more symmetrical and closer to the flat membrane and anode, which minimizes ohmic
357 losses. The angle creates an ohmic drop distribution but the difference in distance is small and all
358 the electrode baffles are at the same distance to the membrane.
- 359 3. Allows convection of fluid on both sides of the electrode, which decreases the diffusion layer
360 thickness and improves mass transfer to and from the cathode surface to the bulk.
- 361 4. Improves convection on the surface of the membrane, which facilitates the movement of
362 protons away from the bipolar membrane where it is generated.
- 363 5. Avoids stagnation and accumulation of particles from the slurry.

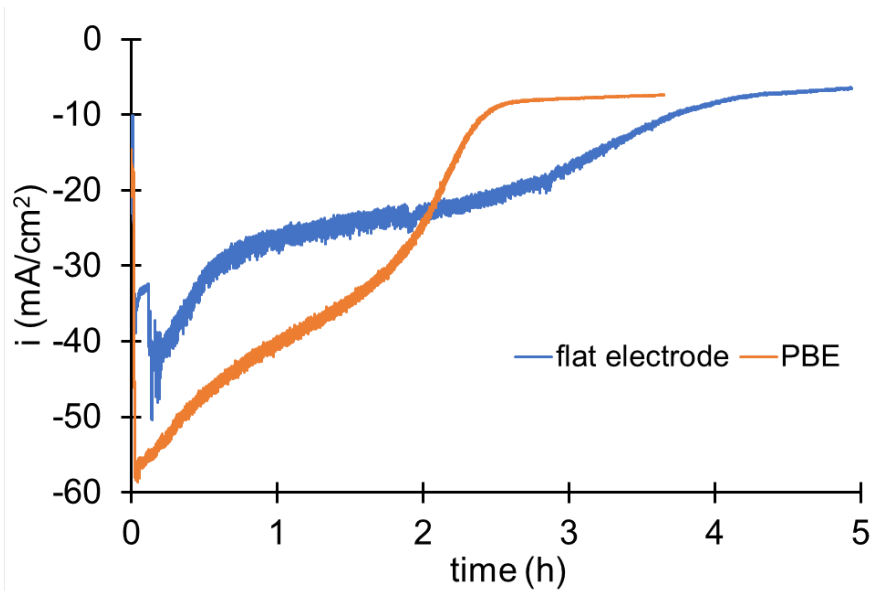
364 The pitch blade impeller provides axial and radial flow of the slurry, and both directions are
365 expected on the cathode surface. The angle of the electrode can be changed from 0 - 90°,
366 although low angles are not of interest since it blocks the flow of slurry between baffles.

367 The current profiles of four different leaching experiments using two different pulp densities and
368 two different baffle geometries are presented in Figure 6. The leaching efficiencies of these
369 experiments were ≥ 97%. The initial temperature was 32 °C and 38 °C before the addition of
370 black mass, through sulfuric acid heat of solution for Figure 6A and Figure 6B, respectively,

371 with a decrease of less than 3 °C during the leaching process.



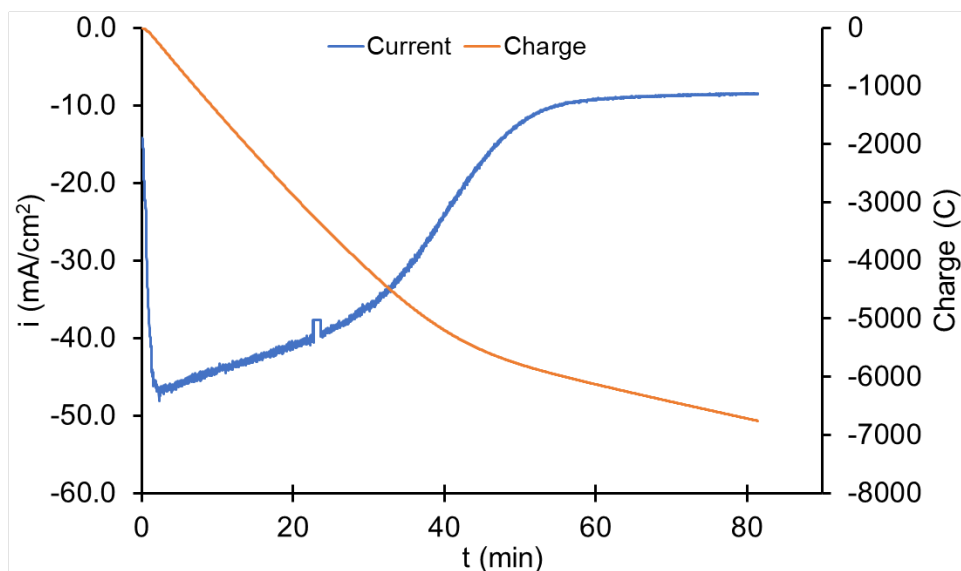
372



373

374 **Figure 6.** Current profile using the single PBE for the leaching of LIBBM with 40 mM of FeSO₄
375 as reductant. **(A, top)** 73 g/L of LIBBM in a 1M H₂SO₄ solution **(B, bottom)** 146 g/L of LIBBM
376 in a 1.7 M H₂SO₄ solution. Stirring in both cases was at 700 rpm. The baffle electrode
377 outperforms the flat electrode with higher currents and shorter leaching times but using the same
378 submerged electrode area of 33 cm².

379



380

381 **Figure 7.** Current profile during the leaching of LIBBM with 40 mM of FeSO₄ as reductant,
 382 with 73 g/L g of LIBBM in a 1 M H₂SO₄ solution with stirring at 800 rpm. A dual BPE reactor
 383 was used, as shown in Figure 1D, with an electrode area of 55.8 cm². The charge to background
 384 current transition is about 6050 C.

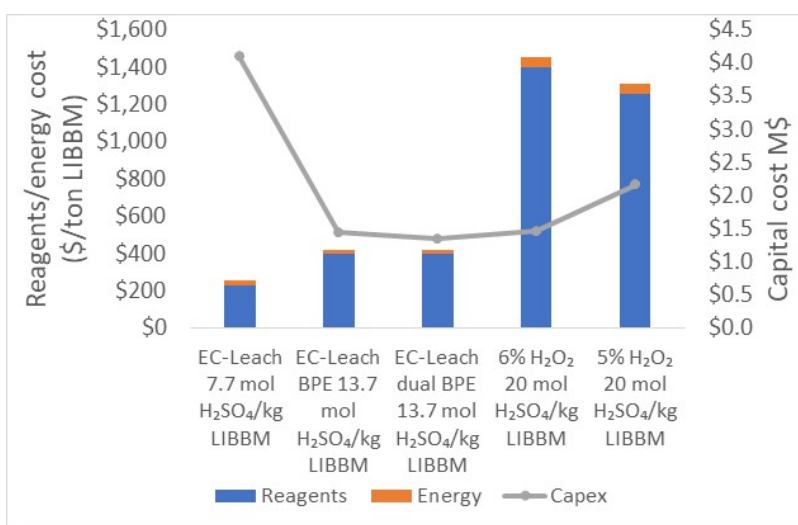
385 The results in Figure 6 show the impact of the electrode geometry on the overall leaching time,
 386 even when the electrode area and approximate position of the electrode is the same, at 73 and
 387 146 g/L pulp densities. The peak current densities obtained for the PBE were 52 and 58 mA/cm²,
 388 respectively.

389 Additionally, a double cathode reactor design was implemented as shown in Figure 1D. The
 390 current density and charge curves appear in Figure 7, with a leaching time of just under an hour,
 391 which is an improvement over the leaching shown in Figure 6A where only one cathode was
 392 used. The main reason for this improvement is the increase in the cathode area, which translates
 393 into an increase in total current. The electrode area to reactor volume ratio (A_c/V) went from
 394 0.183 to 0.310 cm⁻¹. With an electrode face area of 55.8 cm² the peak current density obtained
 395 was 48 mA/cm², which is 6% lower than the peak current density of 51 mA/cm² in Figure 6A. In
 396 the case of the dual BPE, both cathodes are in electrical contact and function as a single cathode,
 397 as well as the anodes. The PBE-Membrane-Anode (PBE-M-A) combination is repeated in the
 398 case of the dual cathode reactor. In a square reactor two more PBE-M-A combinations could still
 399 be added to increase electrode area. Moreover, a higher number of electrode segments could be
 400 added on the same linear distance, resulting in additional area but decreasing the inter-segment
 401 spacing. In future work, optimization of the BPE can be performed by exploring different angles,
 402 spacing and shape of the segmented baffles.

403 **3.4 Technoeconomic analysis TEA**

404 To better elucidate the effects of the system improvements in the economic feasibility of the
 405 electrochemical leaching process, a technoeconomic comparison was performed using the
 406 conditions and methodology described in our previous work [23], where capital, reagents, and
 407 energy costs of the electrochemical leaching are compared against published information for

408 H₂O₂ based leaching process [46, 47]. Figure 8 shows how the leaching time reduction of the
 409 PBE and dual PBE configuration scenarios featured on Figure 6A and Figure 7, respectively,
 410 decrease over 67% the estimated capital cost of the electrochemical leaching when compared
 411 against the reported initial operations at 65 g/L and 7.7 mol of H₂SO₄/kg of LIBBM [23].
 412 Moreover, the estimated capital cost for both PBE and dual PBE are slightly lower than those
 413 estimated for the peroxide leaching scenarios. Assumptions for the cost of the dual PBE
 414 configuration included a 25% increase in material costs, when compared with the single PBE,
 415 considering that a second cathode, membrane, and anode are needed. Nevertheless, the
 416 advantage on operation time outpaces the increase material costs. Higher costs in reagents are
 417 reported for the PBE scenarios as higher acid to LIBBM were used in this study. However,
 418 reagent and energy costs of the electrochemical leaching remain less than 60% of those estimated
 419 for the H₂O₂ based leaching as less acid and no H₂O₂ is used.



420

421 **Figure 8.** Technoeconomic comparison of the effect of processing time reduction on the
 422 electrochemical leaching economic competitiveness against established H₂O₂ based
 423 hydrometallurgical processes.

424 3.5 Electrochemical leaching model

425 Mathematical models of electrochemical reactors [48], and of leaching reactors [49-53], have
 426 been previously reported. To bridge gaps in the understanding of the fundamental processes in
 427 electrochemical leaching of LIBBM and perform simulations that can inform equipment design
 428 and future scale-up of the system, an unsteady-state mathematical model was developed. The
 429 model includes “micro” processes at the leaching particles in the slurry and the electrode surface,
 430 and “macro” mass balances in the reactor.

431 The LIBBM composition is complex and will have a mixture of Li-NMC oxides, apart from
 432 metal particles (Cu, Fe, Al), carbon, graphite, and pieces of battery separators. For this model,
 433 we simplify the active material to a typical NMC or LiCoO₂ chemistry that undergoes the
 434 reaction in Equation 1. Variables are defined in the Nomenclature at the end of the document.
 435 The mol balance of the active material particles is shown in Equations 9-10:

436

437

438 The limiting current at the electrode is:

439

440 The balance of iron at constant volume in the reactor is:

441

442

443 The surface reaction rate is not constant, as it depends on the reductant concentration. For a first-
444 order reaction and if the rate is surface reaction-limited:

445

446 Combining and simplifying equations 12-14 we obtain:

447

448 The area of the particle is a function of its radius or characteristic length, which is in turn a
449 function of time, i.e., $A_p(r(t))$, so Equations 10, 14 and 15 need to be solved numerically.

450 The current goes to a maximum after the LIBMM is added. At this point, the reaction rate on the
451 particles equals the reduction rate at the electrode; the left side of Equation 15 is zero and we
452 have a minimum in the concentration of Fe^{2+} or maximum in Fe^{3+} :

453

454 The second term of the denominator is a dimensionless quantity in the system, which we call λ^* ,
455 that equals the ratio of concentrations at the maximum current point:

456

457 This dimensionless quantity will tend to be large as the total area of particles is orders of
458 magnitude larger than electrode area for common LIBMM pulp densities (50-300 g/L) and
459 particle size (<50 μm), in which case most of the reductant will be oxidized during the first part
460 of the leaching. The phenomenon can be seen in Figure 12 of the publication by Ferron and
461 Henry [26], where the concentration of reductant Fe^{2+} falls below detection limits in the first half
462 of an electrochemically-assisted leaching of MnO_2 ore particles.

463 The maximum current can be estimated with:

464

465 When $\gg 1$, then the previous equation simplifies to

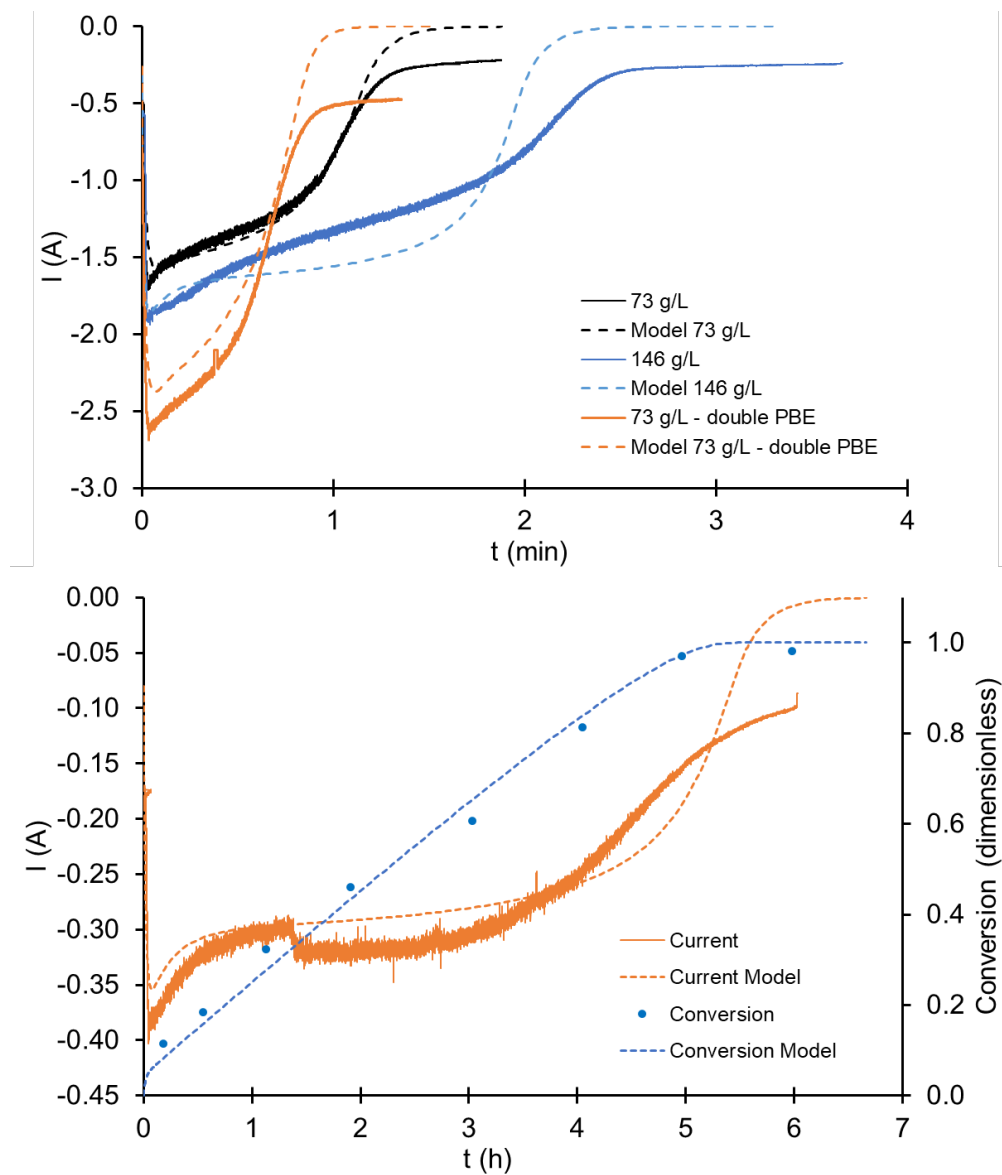
466

467 Which is the maximum current you can get when all the reductant has been oxidized. A value for
468 A_e can be estimated from the actual surface area of a mesh with a formula by Granados et al.[54],
469 so that $A_e = 3.251 \times 33 \text{ cm}^2 = 107.28 \text{ cm}^2$. A value of $k_L = 3.86 \times 10^{-5} \text{ m/s}$ is estimated from
470 Equation 19 and experimental data $I_{max} = 0.8 \text{ A}$, $A_e = 107.28 \text{ cm}^2$, $C_{0Fe2} = 20 \text{ mM}$. For the

471 reduction of Fe³⁺ at limiting current under well-stirred conditions, the following equation applies
472 [39]:

473
474 Using $D = 5 \times 10^{-10} \text{ m}^2/\text{s}$ [36], and the previously estimated value of k_L and Equation 20, a value of
475 $\delta = 0.00129 \text{ cm}$ is calculated, which falls within the order of magnitude of 0.001 cm reported in the
476 literature for the diffusion layer thickness in well stirred reactors [39].

477 COMSOL Multiphysics® 6.1 was used to solve equations 10, 14 and 15 numerically. The
478 parameters were first adjusted to match the 73 g/L leaching with a single PBE and then applied
479 to two other conditions. Table S1 contains the parameters used for the simulation in Figure 9, for
480 three previous runs of electrochemical leaching using the PBE. The model does not incorporate
481 the background current, which is not constant since the experiments were performed at constant
482 voltage and is expected that early in the process there is no appreciable contribution of the HER
483 to the background current, but it becomes important as the Fe³⁺ concentration decreases towards
484 the end of the leaching, as it is apparent in all three experimental runs from Figure 9A. The
485 model does not incorporate particle size distribution effects nor redox reactions between iron
486 ions and metallic aluminum, copper or iron particles present at small concentrations in the
487 LIBBM. The model does include copper plating at limiting current onto the cathode, assuming
488 the Cu concentration in LIBBM reported in Table 1 had already been dissolved. The model
489 successfully approximates the time to completion, which can inform future process design and
490 scale-up. Additionally, the model was adjusted (by changing electrode area and Fe²⁺
491 concentration) to the experiment conditions of Figure 3, showing reasonable agreement in the
492 experimental current profile and the conversion (Figure 9B).



493
 494 **Figure 9. (A, top)** Experimental (solid) and simulated (dotted) current profiles with PBE (single
 495 and double), 40 mM Fe^{2+} . **(B, bottom)** Experimental (solid) and simulated (dotted) current
 496 profile and conversion from Figure 3, using a radial baffle electrode.

497 **3.6 Dimensionless Model**

498 Equations 10,14 and 15 can be combined into a single differential equation:

499

500 The derivatives are then made dimensionless:

501

502

503

504 Equation 21 and its dimensionless version, Equation 24, are non-linear second order differential
505 equations that must be solved numerically, and, to the authors' knowledge, had not been deduced
506 before for the electrochemical leaching of particles. The following dimensionless groups emerge
507 from Equations 23-24:

508

509

510

511 Group λ can be understood as the initial ratio of the surface reaction rate on the particles to the
512 mass transfer-limited rate on the electrode. The next two dimensionless groups are dimensionless
513 times: α is a dimensionless version of the product of mass transport coefficient and electroactive
514 area per unit volume or "volumetric mass transport coefficient", which describes the
515 electrochemical reactor performance normalized to its size and is a useful figure of merit for
516 these types of reactors [45]. For the limit case of an infinite electrode area, $A_e \rightarrow \infty$, groups $1/\alpha$
517 and λ become zero and Equation 24 simplifies to:

518

519 Equation 28 is the equation for the leaching of particles at constant concentration of the leaching
520 agent that is found in the literature [32]. The hypothetical case of an infinite cathode area means
521 C_{Fe2} is kept constant. Group Γ is then the dimensionless initial rate of radius decrease and is
522 equivalent to Crundwell's dimensionless "leaching number" [55].

523 Dimensionless groups are useful for the scale up of the process, as these should be same at
524 different scales. From Γ , if the reductant concentration is doubled, the leaching time is halved, all
525 other parameters being the same. Likewise, from λ if the electrode area to volume ratio is
526 doubled, then the leaching time is halved. The product $\alpha\lambda$ is also a dimensionless group:

527

528 Group $\alpha\lambda$ is the total initial rate of reaction at the leaching particles divided by the reactor
529 volume. From this group, if the number of leaching particles is doubled, then the leaching time is
530 doubled, if all other parameters are kept constant.

531 **4. Conclusions**

532 Electrochemical leaching of LIBBM not only achieves high conversion efficiencies above 96%,
533 but real-time current profiles that are obtained serve as indirect estimation of the leaching rate
534 and end point of the leaching process, without the need of elemental sample analysis.

535 At the Reynold's number used, the kinetic study indicates the leaching rate at the active particles
536 is surface reaction-limited, making the leaching rate susceptible to changes in temperature and
537 reductant concentration at a given acid concentration.

538 Increasing the reductant Fe^{2+} concentration increases the leaching rate and decreases leaching
539 time. This can be achieved by either increasing the initial ferrous sulfate concentration or by

540 increasing the regeneration rate at the cathode through a cathode area increase or an increase in
541 the mass transfer rate. This means that further increases in the leaching rate are possible without
542 increasing the amount of Fe^{2+} added. The new PBE design increases current densities by
543 eliminating the hydrodynamic vortex and improving convection of the slurry on both sides of the
544 electrode when compared to a flat electrode, which decreases the leaching time when compared
545 with a single flat electrode.

546 Sulfuric acid's enthalpy of dissolution from its concentrated reagent can be harnessed directly to
547 increase the leaching rate without external heating. This creates an opportunity for process
548 intensification without additional expense.

549 The numerical model was able to predict the leaching times and estimate the current profiles
550 reasonably well using the new parallel baffle electrode and the radial baffle electrode. It was also
551 able to predict the conversion for the leaching with kinetic study.

552 **5. Nomenclature**

553	c	dimensionless concentration, $C/C_{0\text{Fe}}$
554	i	current density, mA/cm^2
555	k_r	surface reaction first-order kinetic constant, m/s
556	k_L	mass transfer coefficient, m/s
557	n_p	number of particles
558	r	particle radius, m
559	r_0	initial particle radius, m
560		surface reaction rate, $\text{mol}/(\text{m}^2 \cdot \text{s})$
561	t	time, s
562	t_f	time to complete leaching, s
563	A_p	particle area, m^2
564	A_p^*	particle area at the time of maximum current, m^2
565	A_e	electrode area, m^2
566	$C_{\text{Fe}3}$	concentration of Fe^{3+} ions, mol/m^3
567	$C_{\text{Fe}2}$	concentration of Fe^{2+} ions, mol/m^3
568	$C_{0\text{Fe}}$	initial concentration of Fe^{2+} , mol/m^3
569		Diffusivity of iron ions, m^2/s
570	F	Faraday constant, $\text{Coulomb}/\text{mol}$
571	$J_{\text{Fe}2}, J_{\text{Fe}3}$	flux of iron ions, $\text{mol}/(\text{m}^2 \cdot \text{s})$

572	I	electric current, A
573	N	impeller rotation frequency, 1/s
574	N_{NMC}	total moles of NMC particles, moles
575	Re	Reynolds number, dimensionless
576	V	volume, m ³
577	X	conversion, dimensionless
578	Greek	
579		Dimensionless group
580		diffusion layer length, m
581		dimensionless radius, r/r_0
582		dimensionless group
583		dimensionless group at the time of maximum current
584	ρ	molar density of NMC particle, mol/m ³
585		kinematic viscosity, m ² /s
586		dimensionless time, t/t_f
587		dimensionless group

588 Declaration of Competing Interest

589 The authors declare that they have no known competing financial interests or personal
590 relationships that could have appeared to influence the work reported in this paper.

591

592 Acknowledgements

593 The authors acknowledge the financial and technical support of the Critical Materials Institute, an
594 Energy Innovation Hub funded by the U.S. Department of Energy, Office of Energy Efficiency
595 and Renewable Energy, and Advanced Manufacturing Office. The authors would like to thank
596 the Cirba Solutions for providing the black mass materials as well as technical guidance.

597 References

- 598 1. Vieceli, N., et al., *Recycling of Lithium-Ion Batteries: Effect of Hydrogen Peroxide and a*
599 *Dosing Method on the Leaching of LCO, NMC Oxides, and Industrial Black Mass*. ACS
600 Sustainable Chem. Eng., 2023.
- 601 2. Ekberg, C. and M. Petranikova, *Lithium batteries recycling*, in *Lithium process*
602 *chemistry*. 2015, Elsevier. p. 233-267.
- 603 3. Chen, M., et al., *Recycling end-of-life electric vehicle lithium-ion batteries*. Joule,

- 604 2019. **3**(11): p. 2622-2646.
- 605 4. Binnemans, K. and P.T. Jones, *The twelve principles of circular hydrometallurgy*.
- 606 *J. Sustain. Metall.*, 2023. **9**(1): p. 1-25.
- 607 5. Shin, H., et al., *Local oxidation states of Ni, Co, and Mn atoms within pristine*
- 608 *and charged $\text{Li}_x\text{Ni}_0.88\text{Co}_0.08\text{Mn}_0.04\text{O}_2$ primary particles*. *J. Phys. Chem. Solids*,
- 609 2021. **148**: p. 109732.
- 610 6. Meshram, P., B. Pandey, and T. Mankhand, *Hydrometallurgical processing of*
- 611 *spent lithium ion batteries (LIBs) in the presence of a reducing agent with emphasis on*
- 612 *kinetics of leaching*. *Chem. Eng. J.*, 2015. **281**: p. 418-427.
- 613 7. Meshram, P., et al., *Comparision of different reductants in leaching of spent*
- 614 *lithium ion batteries*. *JOM*, 2016. **68**: p. 2613-2623.
- 615 8. Sun, L.-y., et al., *Hydrometallurgical recycling of valuable metals from spent*
- 616 *lithium-ion batteries by reductive leaching with stannous chloride*. *Int. J. Miner., Metall.*
- 617 *Mater.*, 2021. **28**(6): p. 991-1000.
- 618 9. Cerrillo-Gonzalez, M.d.M., et al., *Acid leaching of LiCoO_2 enhanced by reducing*
- 619 *agent. Model formulation and validation*. *Chemosphere*, 2022. **287**: p. 132020.
- 620 10. Gao, W., et al., *Selective recovery of valuable metals from spent lithium-ion*
- 621 *batteries—process development and kinetics evaluation*. *J. Cleaner Prod.*, 2018. **178**: p.
- 622 833-845.
- 623 11. Adhikari, B., et al., *Electrochemical leaching of critical materials from lithium-*
- 624 *ion batteries: A comparative life cycle assessment*. *Resour., Conserv. Recycl.*, 2023. **193**:
- 625 p. 106973.
- 626 12. Lei, S., et al., *Strengthening valuable metal recovery from spent lithium-ion*
- 627 *batteries by environmentally friendly reductive thermal treatment and electrochemical*
- 628 *leaching*. *ACS Sustainable Chem. Eng.*, 2021. **9**(20): p. 7053-7062.
- 629 13. Prabakaran, G., et al., *Electrochemical process for electrode material of spent*
- 630 *lithium ion batteries*. *Waste Manage.*, 2017. **68**: p. 527-533.
- 631 14. Meng, Q., Y. Zhang, and P. Dong, *Use of electrochemical cathode-reduction*
- 632 *method for leaching of cobalt from spent lithium-ion batteries*. *J. Cleaner Prod.*, 2018.
- 633 **180**: p. 64-70.
- 634 15. Liu, K., et al., *Innovative electrochemical strategy to recovery of cathode and*
- 635 *efficient lithium leaching from spent lithium-ion batteries*. *ACS Appl. Energy Mater.*,
- 636 2020. **3**(5): p. 4767-4776.
- 637 16. Jin, W. and Y. Zhang, *Sustainable electrochemical extraction of metal resources*
- 638 *from waste streams: from removal to recovery*. *ACS Sustainable Chem. Eng.*, 2020.
- 639 **8**(12): p. 4693-4707.
- 640 17. Porvali, A., et al., *Lithium ion battery active material dissolution kinetics in Fe*
- 641 *(II)/Fe (III) catalyzed $\text{Cu-H}_2\text{SO}_4$ leaching system*. *Sep. Purif. Technol.*, 2020. **236**: p.
- 642 116305.
- 643 18. Porvali, A., S. Shukla, and M. Lundström, *Low-acid leaching of lithium-ion*
- 644 *battery active materials in Fe-catalyzed $\text{Cu-H}_2\text{SO}_4$ system*. *Hydrometallurgy*, 2020. **195**:
- 645 p. 105408.
- 646 19. Ghassa, S., et al., *The reductive leaching of waste lithium ion batteries in*
- 647 *presence of iron ions: Process optimization and kinetics modelling*. *J. Cleaner Prod.*,
- 648 2020. **262**: p. 121312.
- 649 20. Ghassa, S., et al., *Iron scrap, a sustainable reducing agent for waste lithium ions*
- 650 *batteries leaching: An environmentally friendly method to treating waste with waste*.
- 651 *Resour., Conserv. Recycl.*, 2021. **166**: p. 105348.

- 652 21. Chernyaev, A., et al., *The efficiency of scrap Cu and Al current collector*
653 *materials as reductants in LIB waste leaching*. Hydrometallurgy, 2021. **203**: p. 105608.
- 654 22. Peng, C., et al., *Extraction of Li and Co from industrially produced Li-ion battery*
655 *waste—Using the reductive power of waste itself*. Waste Manage., 2019. **95**: p. 604-611.
- 656 23. Diaz, L.A., et al., *Electrochemical-assisted leaching of active materials from*
657 *lithium ion batteries*. Resour., Conserv. Recycl., 2020. **161**: p. 104900.
- 658 24. Deng, F., et al., *Critical Review on the Mechanisms of Fe²⁺ Regeneration in the*
659 *Electro-Fenton Process: Fundamentals and Boosting Strategies*. Chem. Rev., 2023.
660 **123**(8): p. 4635-4662.
- 661 25. Qiang, Z., J.-H. Chang, and C.-P. Huang, *Electrochemical regeneration of Fe²⁺*
662 *in Fenton oxidation processes*. Water Res., 2003. **37**(6): p. 1308-1319.
- 663 26. Ferron, C. and P. Henry, *The use of ferrous sulphate to enhance the dissolution of*
664 *cobaltic minerals*. Presentation at Hydrometallurgy, 2008.
- 665 27. Faraji, F., et al., *Kinetics of leaching: a review*. Rev. Chem. Eng., 2022. **38**(2): p.
666 113-148.
- 667 28. Mishra, P. and F. Ein-Mozaffari, *Using tomograms to assess the local solid*
668 *concentrations in a slurry reactor equipped with a Maxblend impeller*. Powder Technol.,
669 2016. **301**: p. 701-712.
- 670 29. Pukkella, A.K., et al., *Improved mixing of solid suspensions in stirred tanks with*
671 *interface baffles: CFD simulation and experimental validation*. Chem. Eng. J., 2019. **358**:
672 p. 621-633.
- 673 30. Yanez-Varela, J.A., et al., *Experimental and numerical evaluation of the*
674 *performance of the electrochemical reactor operated with static and dynamic electrodes*
675 *in the reduction of hexavalent chromium*. Chem. Eng. J., 2020. **390**: p. 124575.
- 676 31. Diaz, L.A., et al., *Comprehensive process for the recovery of value and critical*
677 *materials from electronic waste*. J. Cleaner Prod., 2016. **125**: p. 236-244.
- 678 32. Levenspiel, O., *Chemical reaction engineering*. 3rd ed. 1999: John Wiley & Sons.
- 679 33. Fogler, H., *Elements of chemical reaction engineering*. 5th ed. 2020. 243-320.
- 680 34. Faraji, F., et al., *Fungal bioleaching of WPCBs using Aspergillus niger:*
681 *Observation, optimization and kinetics*. J. Environ. Manage., 2018. **217**: p. 775-787.
- 682 35. Grénman, H., T. Salmi, and D.Y. Murzin, *Solid-liquid reaction*
683 *kinetics—experimental aspects and model development*. Rev. Chem. Eng., 2011. **27**(1-2):
684 p. 53-77.
- 685 36. Benari, M. and G. Hefter, *Electrochemical characteristics of the iron (III)/iron*
686 *(II) system in dimethylsulphoxide solutions*. Electrochim. Acta, 1991. **36**(3-4): p.
687 471-477.
- 688 37. Li, L., et al., *Process for recycling mixed-cathode materials from spent lithium-*
689 *ion batteries and kinetics of leaching*. Waste Manage., 2018. **71**: p. 362-371.
- 690 38. He, L.-P., et al., *Leaching process for recovering valuable metals from the*
691 *LiNi^{1/3}Co^{1/3}Mn^{1/3}O₂ cathode of lithium-ion batteries*. Waste Manage., 2017. **64**: p.
692 171-181.
- 693 39. Prentice, G., *Electrochemical engineering principles*. 1991: Prentice Hall
- 694 40. Walsh, F., *Electrochemical technology for environmental treatment and clean*
695 *energy conversion*. Pure Appl. Chem., 2001. **73**(12): p. 1819-1837.
- 696 41. Colli, A.N. and J.M. Bisang, *A CFD study with analytical and experimental*
697 *validation of laminar and turbulent mass-transfer in electrochemical reactors*. J.
698 Electrochem. Soc., 2018. **165**(2): p. E81.
- 699 42. Leenson, I., *Sulfuric acid and water: paradoxes of dilution*. J. Chem. Educ., 2004.

700 **81(7):** p. 991.
701 43. Klaehn, J.R., et al., *Removal of impurity Metals as Phosphates from Lithium-ion*
702 *Battery leachates*. Hydrometallurgy, 2023. **217:** p. 106041.
703 44. Page, J.R., et al., *Recent Progress in Electrochemical Upgrading of Bio-Oil*
704 *Model Compounds and Bio-Oils to Renewable Fuels and Platform Chemicals*. Materials,
705 2023. **16(1):** p. 394.
706 45. Pletcher, D. and F.C. Walsh, *Industrial electrochemistry*. 1990: Springer Science
707 & Business Media.
708 46. Kang, J., et al., *Preparation of cobalt oxide from concentrated cathode material*
709 *of spent lithium ion batteries by hydrometallurgical method*. Adv. Powder Technol.,
710 2010. **21(2):** p. 175-179.
711 47. Kim, S., et al., *Recycling process of spent battery modules in used hybrid electric*
712 *vehicles using physical/chemical treatments*. Res. Chem. Intermed., 2014. **40:** p.
713 2447-2456.
714 48. Rivera, F.F., et al., *Mathematical modeling and simulation of electrochemical*
715 *reactors: A critical review*. Chem. Eng. Sci., 2021. **239:** p. 116622.
716 49. Peters, E., *The mathematical modeling of leaching systems*. JOM, 1991. **43:** p.
717 20-26.
718 50. Lapidus, G., *Mathematical modelling of metal leaching in nonporous minerals*.
719 Chem. Eng. Sci., 1992. **47(8):** p. 1933-1941.
720 51. Dong, L., I. Mazzarino, and A. Alexiadis, *Development of solid–fluid reaction*
721 *models—a literature review*. ChemEngineering, 2021. **5(3):** p. 36.
722 52. Salmi, T., J. Wärnä, and P. Tolvanen, *Understanding of Solid-Fluid Kinetics and*
723 *Mass Transfer: From Ideal to Non-ideal Models, From Perfect Spheres to Moon*
724 *Landscape*. Front. Chem. React. Eng., 2020. **2:** p. 6.
725 53. Crundwell, F., *Progress in the mathematical modelling of leaching reactors*.
726 Hydrometallurgy, 1995. **39(1-3):** p. 321-335.
727 54. Mendoza, P.G., et al., *Liquid–solid mass transfer to a rotating mesh electrode in a*
728 *rotor–stator spinning disc configuration*. Int. J. Heat Mass Transfer, 2017. **104:** p.
729 650-657.
730 55. Crundwell, F., *The leaching number: Its definition and use in determining the*
731 *performance of leaching reactors and autoclaves*. Miner. Eng., 2005. **18(13-14):** p.
732 1315-1324.
733